Status and New Ideas Regarding Liquid Argon Detectors

Alberto Marchionni

Fermi National Accelerator Laboratory, Batavia, Illinois 60510;
email: alberto@fnal.gov

Annu. Rev. Nucl. Part. Sci. 2013. 63:269–90

First published online as a Review in Advance on July 15, 2013

The *Annual Review of Nuclear and Particle Science* is online at nucl.annualreviews.org

This article's doi:
10.1146/annurev.nucl.012809.104445

Keywords

time-projection chamber, detectors, neutrino oscillations, proton decay, astrophysical neutrinos

Abstract

Large (up to ~100 kt) liquid argon (LAr) time-projection chamber detectors are presently being considered for proton decay searches and neutrino astrophysics, as well as for far detectors for the next generation of long-baseline neutrino oscillation experiments that aim to determine neutrino mass hierarchy and search for *CP* violation in the leptonic sector. These detectors rely on the capabilities to assemble large volumes of LAr in ultrahigh-purity conditions, possibly in an underground environment, and to achieve relatively long drifts for the ionization charge. Several proposals have been developed, each of which takes a different approach to the design of the cryogenic vessels and has different scales of modularity to reach the final mass dictated by physics. New detector concepts, with innovative designs of readout electronics and novel methods for the readout of the ionization charge and scintillation light, have been proposed.

Contents

1. INTRODUCTION

The use of a liquid argon (LAr) ionization chamber (1) was first demonstrated in the early 1950s, but not until the end of the 1960s, following a suggestion by Alvarez (2), were liquid noble-gas devices considered candidates for high-energy particle detectors. In 1977, Rubbia (3) proposed a LAr time-projection chamber (TPC) for neutrino detection. Other groups (4, 5) were developing the idea of a LAr TPC at almost the same time.

Thanks to the high mobility (6) and low diffusion (7) of electrons in LAr, large LAr volumes can be operated as TPCs, providing high-quality imaging and high-resolution energy measurements from the detection of the ionization charge (8). The relatively high density of LAr and its commercial availability enable one to assemble large masses of argon suitable for use as both the target and the detector of incoming particles. A LAr TPC is a continuously sensitive detector that can measure, in addition to the ionization charge, the scintillation light (9–11) emitted by excited argon diatomic molecules (excimers) to determine the absolute event time and to provide a self-trigger with no bias on the charge detection. Large LAr volumes can be read out (5) with high spatial granularity (of the order of a few cubic millimeters) by finely instrumenting only two of the three spatial coordinates and, following the TPC principle, using the drift time to measure the third coordinate.

The performance of a LAr TPC critically depends on the amount of electronegative impurities (12–14); impurity concentrations less than a few tens of parts per trillion are required for drift paths of several meters. High argon-purification rates, which are necessary in all large LAr detectors, can be achieved with argon purification in liquid phase, as first discussed in Reference 15.

LAr TPCs overcome the deficiencies of both bubble chambers (which are limited in size and sensitive only for short times) and large-size calorimetric detectors (which suffer from coarse granularity and limitations in the identification of electromagnetic showers). LAr TPCs, thanks to their high readout granularity, can sample electromagnetic showers down to a few percent of a radiation length, making them excellent detectors for electron identification. When compared with water Cherenkov detectors, LAr TPCs permit lower momentum thresholds for the identification of particles that are heavier than electrons, notably protons, and are predicted to provide greater electron-identification efficiency in the presence of a π^0 background.

High-energy physicists quickly realized the potential to use LAr TPCs to detect neutrinos from astrophysical sources, in particular solar neutrinos (16), and more generally to detect very rare events such as proton decay (17). Since the mid 1980s, the ICARUS Collaboration (18–20), led by Rubbia, has submitted a series of proposals to the Gran Sasso Laboratory (LNGS) in Italy for the underground installation of kilotonne-scale LAr TPC modules; at the same time, they initiated a dedicated research and development (R&D) program. The ICARUS Collaboration is currently operating the largest LAr TPC ever built, the ICARUS T600 (21, 22). This instrument, located underground at LNGS and operated in conjunction with the CERN–to–Gran Sasso neutrino beam, has an active mass of ∼500 t, demonstrating the feasibility of using a large LAr installation in an underground environment.

Detectors (23–30) ranging from the 10-kt scale up to 100 kt have been proposed for future experimental programs that would combine proton decay searches, observation of atmospheric and supernova neutrinos, and long-baseline neutrino oscillation physics. Such programs would optimally exploit the features of LAr TPC detectors, which are ideally suited for making measurements in the MeV-to-GeV range and demonstrate superior performance in electron identification. Clean electron measurements are crucial in long-baseline neutrino oscillation experiments, with conventional wide-band neutrino beams, for measurements of the $\nu_\mu \rightarrow \nu_e$ transition probability, the determination of the neutrino mass ordering, and especially searches for *CP* violation in the leptonic sector (31).

A 10-kt-scale LAr detector, if installed underground even at a moderate depth, would extend the search for proton decay via modes favored by supersymmetric grand unified models (e.g., $p \rightarrow K^+\bar{\nu}$) above $\sim 10^{34}$ years. Such a detector would have between 5 and 10 times the efficiency of water Cherenkov detectors for such decays (32).

Core-collapse supernova neutrinos can be detected by LAr TPCs through different channels (33), namely elastic scattering on atomic electrons and neutral- and charged-current processes on argon according to the neutrino flavor. The possibility of observing supernova relic neutrinos was considered in Reference 34.

Direct observation of the τ neutrino component in atmospheric neutrinos with a LAr TPC was first suggested in Reference 35 and more recently discussed in Reference 36. LAr TPCs, possibly magnetized (23, 37), have also been proposed for use in neutrino factory beams (23, 38) to identify, in addition to muons, final states with electrons and τ leptons. More recently, LAr TPCs have been proposed (39, 40) for use as detectors in short-baseline experiments for neutrino cross-section measurements and in searches for sterile neutrinos. The low-energy frontier in LAr, down to energies of tens of keV, is being actively explored by direct dark matter search experiments (41). A size increase of a factor of 10 to 100 with respect to the present ICARUS T600, although challenging, is not unrealistic, as we argue below.

In Section 2, we provide a historical overview of LAr technology; Section 3 summarizes the thermal and physical properties of LAr. In Section 4, we discuss in detail the main issues in scaling from an ICARUS-like detector to a tens-of-kilotonnes device and describe ongoing

R&D. Different design concepts, as well as intermediate-scale detectors and test-beam setups, are reviewed in Section 5. In Section 6, we present our conclusions.

2. HISTORICAL OVERVIEW OF LIQUID ARGON TECHNOLOGY

Long ago, researchers recognized that ionizing radiation in LAr can excite electrons into conduction levels so that they can be transported through the liquid by an applied electric field. At the end of the 1940s, initial observations (42–45) of conductivity pulses in LAr demonstrated high electron mobility; these observations led to calorimetric measurements of ionizing radiation (1).

In 1968, Alvarez (2) suggested that liquid noble-gas detectors could be used as high–spatial resolution detectors, given the expected low diffusion of electrons in liquid, and as total absorption counters with good energy resolution. This proposal led to the development of a multistrip LAr ionization chamber with a better position resolution than that of gas detectors (7). This instrument also provided the first measurement of electron diffusion in LAr.

At the end of the 1960s, Doke (see Reference 46 for a historical review of early R&D on noble liquids) began taking comprehensive measurements on the fundamental properties of LAr and liquid xenon as detector media. At approximately the same time, to mitigate the unsuccessful attempts to achieve charge amplification in LAr (47) and obtain relatively large signals, Dolgoshein et al. (48, 49) proposed and successfully tested the main features of double-phase argon detectors, in which ionization electrons produced in the liquid are extracted to the argon vapor on top and are there amplified.

In 1974, aiming to create a high-energy particle detector with good energy resolution, Willis & Radeka (50) built and operated a LAr ionization chamber with a large number of thin metallic plates acting as readout electrodes. They employed specifically developed low-noise electronics that were optimized for large capacitances. Rubbia's (3) 1977 proposal of a LAr TPC gave rise to the concept of a detector that could act simultaneously as a homogeneous calorimeter and as a tracking device and would have an imaging quality comparable to that of a bubble chamber.

In a TPC, ionization electrons drift from a cathode toward a readout structure by means of a uniform electric field (51) to achieve a constant drift velocity. The electric field is generated by surrounding the drift volume by a set of equally spaced electrodes, denoted field shapers, that are kept at distinct potentials such that the difference in voltage between two contiguous electrodes is constant.

Reference 5 describes the standard method for reading out the ionization charge in LAr TPCs. This method, pioneered by the ICARUS Collaboration, employs three parallel wire planes immersed in LAr, with wires at different angles. By properly biasing the wire planes, the first two wire planes become fully transparent to the drifting electrons and can detect a signal induced by the moving electrons, whereas the last plane acts as a collecting electrode. The signals (see Reference 21 for a sketch of the signal shapes) are digitized at a frequency of a few megahertz. Each wire plane provides a two-dimensional view of the event; one coordinate is given by the wire number and the other by the drift time.

2.1. Liquid Argon–Purification Techniques

The LAr TPC concept requires drift paths of at least several tens of centimeters. This constraint imposes strict limits on the concentration of electronegative impurities in LAr (see Section 3.4).

Two experimental groups initiated investigations into argon-purification systems and long drift lengths. The Chen group (4, 52) first achieved electron attenuation lengths of ~35 cm with drift fields of 1 kV cm^{-1}. A large-scale argon-purification system (53) employed gas- and

liquid-phase purification by using reduced copper and a mixture of molecular sieves (4A, 5A, and 13X), respectively, in a closed-loop recirculation of the evaporated argon. This system attained attenuation lengths $\geq$3.7 m at drift fields of 0.5 kV cm^{-1}, which correspond to an impurity level of $\leq$0.2 ppb oxygen equivalent.

The Rubbia group (54, 55) investigated electron lifetimes in small, gridded ionization chambers, operated at very low drift fields, by analyzing signal pulse shapes. The purification system, operated in the gas phase, employed a mixture of molecular sieves and silica gel to remove water, carbon dioxide, and hydrocarbons, along with a commercial Oxisorb® getter,[1] made of reduced chromium oxide on a silica gel carrier, to absorb oxygen. A 10-cm drift chamber was operated (54) at drift fields down to 10 V cm^{-1}; the drift times were 1.8 ms.

Subsequently, a chamber with a 153-mm drift gap and drift fields as low as 5 V cm^{-1} attained electron lifetimes of ~9 ms (55), which correspond to an impurity concentration of 0.03 ppb oxygen equivalent. This development led to the creation of electron lifetime detectors (56). These detectors were based on attenuation measurements of electrons, extracted by a Nd:YAG UV laser beam from a metallic photocathode, in a double-gridded drift chamber. The ability to purify LAr directly in liquid phase (15) by use of a combination of molecular sieves and Oxisorb cartridges demonstrated the feasibility of employing the ultrapure-LAr technique over very large volumes.

2.2. Development of Liquid Argon Time-Projection Chamber Detectors

The bidimensional tracking capabilities of a LAr TPC were first demonstrated by Chen and colleagues (57), who used drift distances of up to 25 cm and a multistrip readout anode with a 2.5-mm pitch. Increasingly large detectors have been constructed and tested by the ICARUS Collaboration over the past 20 years. A two-dimensional LAr TPC (58) with a 24-cm drift gap, the first to be equipped with a sense-wire (induction) plane to demonstrate nondestructive detection (5) of the electron image produced by ionizing events, was exposed to a 5-GeV pion beam at the CERN PS and used to study low-energy electrons by observations of the associated δ-rays.

For the first time, a 3-t LAr TPC (59, 60), with a maximum drift distance of 42 cm, produced three-dimensional images of ionizing events over a volume of ~1.5 m^3. A screening grid was followed by two 2-mm-pitch wire planes that worked in induction mode and collection mode. Given the small ionization charge signal released in LAr by a minimum ionizing particle (MIP) (see Section 3.2), the use of low-noise readout electronics is required (see Section 4.4.1). This 3-t LAr TPC employed charge-sensitive preamplifiers with a junction field effect transistor (JFET) input stage in an unfolded cascade architecture (61).

In the 1990s, the ICARUS–Milano Collaboration pioneered the use of LAr TPCs as neutrino detectors with the exposure of a 50-liter chamber on the CERN West Area Neutrino Facility (62). The front-end electronics (63) were based on JFETs operated in LAr close to the readout wires, which minimized the preamplifier input capacitance due to the absence of long readout cables.

The detection of scintillation light in coincidence with ionizing tracks in a LAr TPC (64) can be used as an absolute time measurement for the spatial localization of the ionizing event. Conventional glass-window photomultiplier tubes (PMTs) are not sensitive to the far-vacuum UV light produced in LAr, which would require the use of costly PMTs with MgF_2 windows. A suitable solution (65) makes use of glass-window PMTs immersed in LAr; these PMTs were developed specifically for use at cryogenic temperatures and are coated with a fluorescent wavelength shifter (66) to the PMT-sensitive region.

[1]Manufactured by Messer–Griesheim GmbH, Krefeld, Germany.

The construction of the ICARUS T600 detector (21) was an important step in detector size. This detector is composed of a large cryostat split into two identical, adjacent 300-t modules, each of which has an internal volume of $3.6 \times 3.9 \times 19.6\ m^3$. The ionization charge is detected via wire chambers and scintillation light by an array of 74 PMTs (67). The TPC wire chambers are positioned on the opposite sides of a cathode plane placed in the middle of each 300-t module. Each wire chamber has three parallel wire planes with 3-mm wire pitch and wires at 0° and $\pm 60°$, with respect to the horizontal direction; the wires are read out by low-noise warm electronics located outside the cryostat (see Section 4.4.1). With a maximum drift distance of ~1.5 m, a cathode voltage of 75 kV is required for a nominal electric field of $500\ V\ cm^{-1}$. A cryogenic, custom-made, high-voltage (HV) feedthrough carries the HV generated by an external power supply to the inside of the cryostat on the cathode plane. It successfully operated up to a maximum of 150 kV (21).

Argon purification is accomplished by both gas and LAr recirculation through Oxisorb getters and molecular sieves. For each 300-t module, the liquid is recirculated by means of an immersed cryogenic pump placed inside an independent dewar. This setup recirculates the full volume in 6 days.

A 300-t module was first operated on the surface; it recorded cosmic-ray data for a period of ~2 months. The electron lifetime reached a value of 1.8 ms and was still increasing by the end of the run (68).

The successful installation of the ICARUS T600 detector (22) in the LNGS underground laboratory was a major milestone in LAr TPC technology. The detector is presently collecting data with a good electron lifetime—up to 7 ms—and it is being used to study neutrino physics (69–71).

3. PROPERTIES OF LIQUID ARGON

Argon, produced industrially by the fractional distillation of liquid air, is readily commercially available, given that it constitutes 1.28% of air by weight. Annual US production alone amounts to ~1,000 kt per year.

The main isotopes of argon (72) are ^{40}Ar (99.6%), ^{36}Ar (0.34%), and ^{38}Ar (0.06%), all of which are stable against radioactive decays. The long-lived radioactive isotope ^{39}Ar, a β emitter with $T_{1/2} = 269$ years and a Q value of 565 keV, is also present in atmospheric argon because it is produced by cosmic rays via the $^{40}Ar(n,2n)\ ^{39}Ar$ process. Measurements in a two-phase argon chamber (73) demonstrate the ^{39}Ar-specific activity of $(1.01 \pm 0.08)\ Bq\ kg^{-1}$ of natural argon; this finding is consistent with a previous determination (74) in atmospheric argon.

Tables 1 and **2** present the main thermal and physical properties of LAr. In the following subsections, we briefly discuss the relevant physical processes for a LAr TPC.

3.1. Scintillation

A charged particle crossing LAr causes ionization and excitation of the argon atoms, yielding free electrons and the emission of scintillation light. Scintillation light is observed (9, 78) in the vacuum UV range in a band centered at 127 nm, with a full width at half maximum (FWHM) of ~10 nm, and is attributed to the emission of excited diatomic molecules (excimers). Transitions from the low excited singlet ($^1\Sigma_u^+$) and triplet ($^3\Sigma_u^+$) molecular states to the ground state have been measured (10) to have decay times of 7 ns and 1.6 μs, respectively; these decay times are independent of the density of ionization. Instead, the intensity ratio of singlet to triplet molecular states depends on the ionization density (10): 0.3 for 1-MeV electrons and 3.0 for fission fragments.

Ionization recombination takes place soon after the initial ionization charge around the trajectory of the ionizing particle is produced, depending on the ionization density and the value of the electric field in LAr. It effectively transforms ionization into scintillation. Excimers form (11)

Table 1 Thermal properties of liquid argon (75, 76)[a]

	Pressure (kPa)	Temperature (K)	Density (g cm^{-3})
Triple point	68.891 ± 0.002	83.8058	—
Liquid phase	100.0	85	1.410
Saturation properties	88.110	86	1.403 (liquid) 5.080 × 10^{-3} (vapor)
NBP	101.325	87.303 ± 0.002	1.395 (liquid) 5.774 × 10^{-3} (vapor)
	109.01	88	1.391 (liquid) 6.174 × 10^{-3} (vapor)
Critical point	4,863 ± 3	150.687 ± 0.015	0.5356 ± 0.0010
At NBP			
Isobaric heat capacity (C_p)	1.117 kJ (kg K)$^{-1}$		
Thermal conductivity	0.1256 W m^{-1} K^{-1}		
Latent heat of vaporization	161.1 kJ kg^{-1}		
Viscosity	270.7 μPa s		
Expansion ratio liquid (NBP) to gas (1 atm, 20°C)	840 vol/vol		

[a]Atomic number, 18; atomic mass, 39.948. Abbreviation: NBP, normal boiling point.

through collisions between either excited atomic states and other atoms in the ground state or ionized atoms and ground-state atoms in a sequence of steps involving recombination with electrons. Approximately 70% of the scintillation induced by 1-MeV electrons without any applied electric field comes from the recombination process, as the authors of Reference 87 measured by simultaneously detecting a decrease in scintillation intensity and an increase in collected electrons while raising the intensity of the electric field.

The average energy required for the production of one photon in LAr has been estimated (11, 88), for 1-MeV electrons with no electric field, to be $W_{ph} = 25$ eV, which is comparable to that for NaI(Tl) crystals. These properties make LAr an excellent scintillator. For an electric field of 300 V cm^{-1}, the reduction in scintillation is ∼35% (64).

The first measurements (89) of the attenuation length of scintillation light in LAr itself yielded $\lambda_{att} = 66 \pm 3$ cm. Researchers suggested (89) that this attenuation is due to Rayleigh scattering in LAr, which was calculated (84) to be 90 ± 32 cm at the peak scintillation wavelength of LAr. Density fluctuations of LAr would greatly enhance Rayleigh scattering. Recently, the attenuation of UV light in LAr, wavelength-resolved in an interval from 118 to 250 nm, was measured (90) to be λ_{att} (127 nm) = 140 cm, with an error of ∼30%. This value is marginally compatible with the previous measurement (89). For large-scale detectors employing LAr scintillation light, this is a critical quantity that merits further investigation.

3.2. Ionization

The average energy required to produce an electron–ion pair in LAr is $W_i = 23.6 \pm 0.3$ eV (8), a value that comes from the saturated collected charge from ^{207}Bi conversion electrons at high electric fields. This value is smaller than that obtained in gaseous argon [$W_g = 26.4$ eV (91)], indicating the presence of a conduction band in the condensed state (8).

Charge recombination measurements in LAr on low-energy ($\lesssim$1-MeV) electrons, as a function of the electric field, have been reported (6, 92–94). Recombination effects for muons and protons

Table 2 Physical properties of liquid argon

Passage of particles	
Stopping power $\langle dE/dx \rangle$ (MIP) (77)	1.508 MeV cm^2 g^{-1}
Nuclear interaction length (77)	119.7 g cm^{-2}
Mass attenuation coefficient for 1-MeV γ (72)	5.762 $\times$ 10^{-2} cm^2 g^{-1}
Critical energy (electrons) (77)	32.84 MeV (for e^-) 31.91 MeV (for e^+)
Radiation length (77)	19.55 g cm^{-2}
Molière radius (77)	12.62 g cm^{-2}
W_i (average energy per ion pair, 1-MeV e^-) (8)	23.6 $\pm$ 0.3 eV
W_{ph} (average energy per photon, 1-MeV e^-) (11)	25 eV
Peak vacuum UV scintillation wavelength (9, 78)	127 nm
Scintillation decay time constants, with relative proportions for 1-MeV e^- (10)	$t_{fast} = 7 \pm 1$ ns (23%) $t_{slow} = 1.6 \pm 0.1$ μs (77%)
Electrical and optical properties	
Ionization energy (gas) (72)	15.7596 eV
Ionization energy (liquid, computed) (79, 80)	13.6–13.8 eV
Dielectric strength (Au–Au electrodes) (81)	~750 kV cm^{-1}
Static dielectric constant (NBP) (82)	1.504
Refractive index (NBP, 435.8 nm) (83)	1.2325
Refractive index (128 nm, computed) (84)	1.38
Free electron properties	
e^- drift velocity (500 V cm^{-1}, 89 K) (68, 85)	1.55 mm μs^{-1}
D_L (drift field 100–350 V cm^{-1}) (60)	4.8 $\pm$ 0.2 cm^2 s^{-1}
D_T (drift field 1–10 kV cm^{-1}) (7, 86)	~13–18 cm^2 s^{-1}

Abbreviations: MIP, minimum ionizing particle; NBP, normal boiling point.

for low drift electric fields (0.2–0.5 kV cm^{-1}) have been measured as a function of the stopping power $\langle dE/dx \rangle$ by the ICARUS 3-t and T600 detectors (60, 95).

Different recombination models have been proposed (93, 96, 97). Following Reference 1, the Jaffé (96) "columnar" model is approximated by the same expression as the so-called Birk's law describing the quenching effects in scintillators: $Q/Q_0 = (1 + k_E/\mathcal{E})^{-1}$, where Q is the collected charge, Q_0 is the initial ionization charge, $\mathcal{E}$ is the electric field, and k_E is a constant to be obtained from a fit to data. This expression does not seem to adequately fit the data of Reference 92 over the full range of electric fields, but it has been successfully used for high electric fields (6, 92, 94).

An explicit dependence on the stopping power $\langle dE/dx \rangle$ and a normalization constant have been introduced (95):

$$Q = A \frac{Q_0}{1 + k/\mathcal{E}\langle dE/dx \rangle},$$

where A and k are parameters to be fit. This phenomenological expression, when fit to the ICARUS 3-t data (60) for drift electric fields from 0.2 to 0.5 kV cm^{-1}, yields (95) $A = 0.800 \pm 0.003$ and $k = 0.0486 \pm 0.0006$ kV cm^{-1} g (cm^2 MeV)$^{-1}$. For MIPs, this expression predicts a remaining charge after recombination equal to 70% and 75% of the initial ionization charge for electric fields of 0.5 kV cm^{-1} and 1 kV cm^{-1}, respectively. In a field of 0.5 kV cm^{-1}, an ionization charge of ~10 fC cm^{-1} of track length is expected for MIPs (**Table 2**).

The so-called box model (93) predicts

$$Q = Q_0 \frac{1}{\xi} \ln(1 + \xi),$$

where ξ is a parameter that is proportional to the ionization charge density and inversely proportional to the electric field. This expression has been successfully used (93, 98) to fit the dependence of charge recombination for low-energy electrons as a function of an electric field up to 10 kV cm^{-1}. Given the importance of the recombination phenomenon for LAr, which directly affects the discrimination of particle types on the basis of their stopping power and the achievable energy resolution, additional measurements of this effect would be welcome.

The intrinsic energy resolution of 1-MeV electrons in LAr has been measured (94), through the detection of the ionization charge, to be 2.7% (FWHM). This value is still a factor of two poorer than the Poisson statistical limit and a factor of seven poorer than the Fano limit (99). The loss of resolution has been explained (98) by the statistical fluctuations in the number of soft δ-rays along the electron track; these δ-rays suffer from larger recombination than do higher-energy electrons.

3.3. Drift and Diffusion

The drift velocity of electrons in LAr depends primarily on the electric field strength (6). A weaker dependence on the temperature has been measured (85). The addition of small amounts of impurities to LAr causes the drift velocity to increase (6). Precise measurements of the drift velocity as a function of the drift electric field and the temperature of the liquid have been performed (85) for electric fields $\mathcal{E}$ and temperatures T in the ranges between 0.5 kV $cm^{-1} \leq \mathcal{E} \leq 12.6$ kV cm^{-1} and 87 K $\leq T \leq 94$ K, respectively. A relative accuracy of $\lesssim 2\%$ was obtained for fields <4 kV cm^{-1}. The mean value of the temperature dependence of the drift velocity, v_d, has been measured to be $\Delta v_d/(\Delta T\, v_d) = (-1.72 \pm 0.08)\%K^{-1}$. The ICARUS Collaboration (68) has performed measurements of the drift velocity for electric fields as low as 60 V cm^{-1} and up to 1 kV cm^{-1} at $T = 89$ K. These values agree well with those from Reference 85 in the overlap region.

Knowledge of the diffusion coefficient D is especially important for long drift times because it directly affects the accuracy of the drift-time measurement and the transverse smearing of the reconstructed tracks. The spread of an isolated group of electrons increases with drift time t with $\sigma = \sqrt{2Dt}$. For gases, the diffusion coefficient in a direction parallel to an electric field (D_L) differs from that in the transverse direction (D_T) (100). For argon gas, D_L is substantially lower than D_T.

Diffusion measurements of electrons in LAr are scarce. An initial measurement (7) yielded $D_T \simeq 13$ cm^2 s^{-1} for a drift field of 2.7 kV cm^{-1}. The mean agitation energy of electrons in LAr, $\langle\epsilon\rangle$, was estimated (86) through the ratio $\langle\epsilon\rangle = e\,D/\mu$ of the diffusion coefficient to mobility μ by measuring the lateral spread of a group of electrons in a parallel-plate ionization chamber operated with electric fields between 2 and 10 kV cm^{-1}. The derived values for D_T lie in a range between ~15 and 18 cm^2 s^{-1}. The value of D_L for low drift fields, ~100–350 V cm^{-1}, was determined (60) by an analysis of the rise time of the electron collection signal; the result, $D_L = 4.8 \pm 0.2$ cm^2 s^{-1}, agrees reasonably well with the Einstein relation for thermal electrons: $eD/\mu = kT$.

3.4. Electron Attachment to Impurities

Following Reference 14, in the presence of electronegative impurities, the concentration of free electrons, $[e]$, in LAr decreases exponentially with time, according to

$$\frac{d[e]}{dt} = -k_s[S][e] \Rightarrow [e] = [e_0]e^{-k_s[S]t} = [e_0]e^{-t/\tau_e},$$

where [S] is the concentration of electronegative impurities, k_s is an electron attachment rate constant, and $\tau_e = 1/(k_s[S])$ is the electron lifetime. Knowledge of the effect of oxygen is particularly important because it is one of the main contaminants in commercial LAr. The attachment rate constants to oxygen have been measured (14) as a function of the electric field strength. For electric fields of less than a few hundred volts per centimeter, the result is $k_{O_2} = 9 \times 10^{10}$ liter mole^{-1} s^{-1} = 3 ppm^{-1} μs^{-1}, which corresponds to $\tau_e(\mu s) \simeq 300/[O_2]$ (ppb). For increasing electric fields, the attachment rate constant decreases, as already observed (12). At an electric field of 1 kV cm^{-1}, $\tau_e(\mu s) \simeq 500/[O_2]$ (ppb).

The mean free path length λ of electrons in LAr was measured (13) to be inversely proportional to the O_2 concentration and linearly proportional to the drift electric field, $\mathcal{E}$, for small values of the electric field: $\lambda = \alpha\mathcal{E}/[O_2]$, where $\alpha = (0.15 \pm 0.03)$ ppm cm^2 kV^{-1}. For low–electric field electron mobilities, namely $\sim$500 cm^2 V^{-1} s^{-1} (55), this value is equivalent to the above expression for the electron lifetime.

3.5. Liquid Argon–Vapor Interface

The characteristics of electron emission from the liquid (48, 49) have been experimentally studied (101, 102). These investigations confirmed the existence of a negative energy level of conduction electrons in LAr of $\sim$0.1 to 0.2 eV (80, 101, 103). The emission of the electrons can be described by the Schottky model of electric field–enhanced thermionic emission.

4. CHALLENGES FOR LARGE LIQUID ARGON DETECTORS

Operation of a tens-of-kilotonnes LAr TPC detector could answer many fundamental physics questions. Doing so would require more than a factor-of-10 increase in size from the present ICARUS T600 detector. The main factors that have been considered in extrapolations to larger detectors include larger cryogenic vessels, longer drift paths to minimize the number of electronic channels per unit volume, lower-cost electronics (possibly located next to the readout elements and immersed in LAr), novel readout methods for ionization charge and scintillation light, and new schemes for the generation of high voltages in LAr. The achievable purity of LAr remains a main design parameter for a LAr TPC. **Figure 1** summarizes these main design considerations and the relationships among them. Monitoring and calibration of the detector performance parameters, such as the purity of the argon and the uniformity of the drift region, are also of primary importance.

4.1. Cryogenic Vessels

The envisioned future detectors require large cryogenic vessels ($\gtrsim$10,000 m^3), suitable for underground construction and operation, that are sufficiently tight to keep electronegative impurities within a few tens of parts per trillion and with low-enough thermal losses to afford the costs of long-term cryogenic operation. Traditionally, high-purity LAr vessels were built as stainless-steel vacuum-insulated dewars, in which the inner vessel is also evacuable. Such devices, if built with standard techniques, are not scalable to the required dimensions of the envisioned LAr detectors. In Section 5.1, we describe a design that aims to maintain the features of vacuum insulation and evacuable vessels for very large containers.

The ICARUS T600 vessel utilizes a cryostat made of two identical, adjacent, evacuable aluminum vessels, each of which contains 300 t of LAr that are thermally insulated by evacuated honeycomb panels (21, 22). The detector is cooled by pressurized liquid nitrogen, which circulates in a thermal shield placed between the insulation panels and the aluminum vessels.

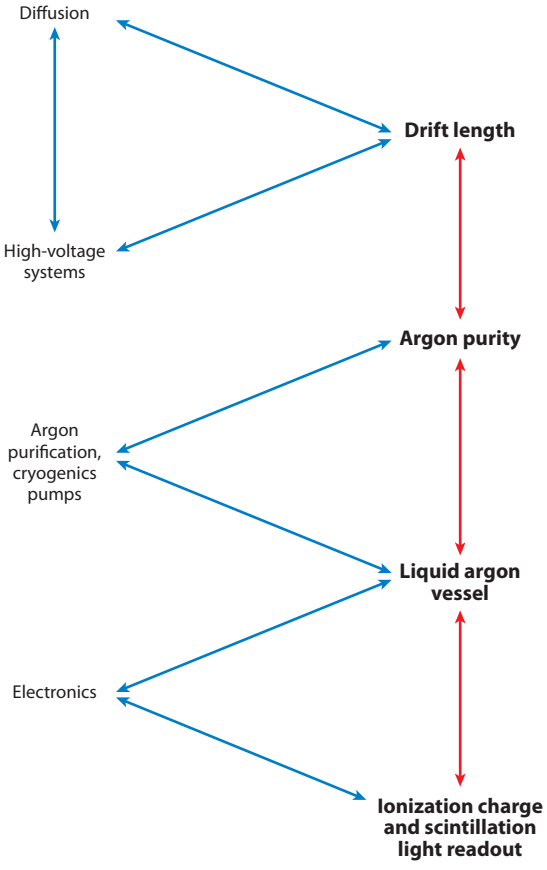

Figure 1

Main design topics for liquid argon time-projection chambers.

Very large cryogenic vessels would hardly be evacuable. In Section 4.3.1, we show that this limitation does not necessarily preclude the necessary LAr purity. Moreover, a high volume-to-surface ratio is advantageous for keeping the detector in cryogenic conditions, for allowing passive insulation, and for maintaining the purity of the argon. Industrial tanks used to contain liquefied natural gas (LNG, which comprises more than 90% CH_4) (104), up to volumes of 200,000 m^3, are built as nonevacuable nickel-steel tanks; perlite is used as thermal insulation. Several groups (24, 25, 105) have proposed the use of such vessels for the containment of LAr, given that the boiling points of LAr and CH_4 are similar (87.3 and 111.6 K, respectively) and the latent heat of vaporization per unit volume is the same for both liquids within 5%. Thermal losses of $\sim$5 W m^{-2} can be achieved with passive insulation methods (i.e., with $\sim$1.5-m-thick perlite insulation). The resulting boil-off of LAr, only $\sim$0.05% per day for a 100-kt LAr vessel, would then be recondensed and returned to the cryostat.

A different solution, again borrowed from the field of LNG technology, has been adopted for the LAr detector of the LBNE project (106) at Fermi National Accelerator Laboratory (FNAL). This system employs a commercial membrane cryostat technology, used in LNG tanker ships (107), that involves a $\sim$1-mm-thick corrugated stainless-steel liner to contain the cryogenic liquid and relies on the surrounding rock to provide mechanical support. A secondary thin aluminum

membrane, serving as secondary containment, is embedded in a 0.8-m-thick passive insulation of solid, reinforced polyurethane foam. The heat input from the surrounding rock is expected to be ~7 W m^{-2}, which causes continuous evaporation of the argon because the cryostat is not directly cooled in this design. Fluid dynamics simulations show the onset of convective currents throughout the entire LAr bath, with speeds of a few centimeters per second, that help limit the temperature gradient across the whole volume to much less than 0.1 K, so the variation of the drift velocity is less than 0.1% (see Section 3.3). The evaporated argon is recovered, recondensed by liquid nitrogen refrigerators, purified, and returned to the cryostat.

4.2. High-Voltage Generation and Feedthroughs

The development of HV systems is crucial for LAr TPCs, which need a stable and uniform drift field over extended LAr volumes. Typically, a drift field of 500 V cm^{-1} is utilized. There are clear advantages in operating a LAr TPC at a higher drift electric field, including shorter charge-collection times, which reduce the attenuation of ionization electrons due to electronegative impurities; lower recombination of the initial ionization charge, particularly for heavily ionizing particles; and lower attachment cross sections of electrons to O_2 impurities (as mentioned in Section 3.4). However, a high drift field may increase the diffusion process and lead to very high voltages on the cathode. It may also require unacceptably high voltages on the charge readout structure to ensure transparency for the collection of the ionization charge.

The HV configuration chosen for ICARUS T600, described in Section 2.2, allows access to the HV power supply for possible repairs, as well as continuous monitoring of the voltage from the current flowing in the resistive voltage divider. The design of the HV feedthrough, operated at a maximum voltage of 150 kV, is in principle scalable to higher voltages, as long as suitable HV power supplies and cables are available.

An alternative solution (108–110) is to build a Cockcroft–Walton voltage multiplier immersed in LAr; the different stages of the multiplier would be directly connected to the field shaper electrodes and to the cathode, thereby avoiding the need for a resistive voltage divider. Because in this case a negligible current is drawn, the voltage multiplier can be operated at a relatively low frequency charging voltage, well outside the relevant bandwidth of the readout electronics. In principle, this concept allows one to reach HV values above the range of commercially available power supplies. A proof of principle is provided in Reference 110, which describes, in detail, the design, characteristics, and operation of a voltage multiplier with 30 stages that is driven by a 50-Hz ac charging voltage supply up to a maximum driving voltage of $V_{pp} = 2$ kV, peak to peak. This device was successfully operated up to a voltage of ~35 kV.

Recently, a voltage multiplier (109) with 125 stages, driven by a maximum ac voltage of $V_{pp} = 4$ kV, peak to peak, was stably operated at a voltage of up to ~120 kV. Discharges encountered at higher voltages are presently under investigation.

Voltage multipliers with many stages are affected by a so-called shunt capacitance because of the capacitance of the diodes and the stray capacitance determined by the geometry of the circuit. These factors cause the output voltage to increase less than linearly with the stage number, even with no current load (108, 110). Designs for up-to-megavolt systems have been discussed (108).

4.3. Liquid Argon Purity and Purification Methods

The purification of LAr, down to electronegative impurity concentrations of a few tens of parts per trillion, and the maintenance of such conditions over many years are key to the successful operation of large LAr TPCs. Continuous recirculation and purification of LAr are necessary in

such detectors, as demonstrated by ICARUS. Argon purity remains an important area of study for R&D, which focus primarily on achieving purity in nonevacuable vessels, on argon-purification techniques, on the qualification of materials used in detector construction, and on monitors of argon purity.

4.3.1. Nonevacuable vessels. In many designs of large LAr TPCs, the cryogenic vessel is nonevacuable and requires the removal of air before it can be filled with LAr. Preliminary tests have been conducted on small tanks (111, 112) of a few cubic meters in the gas phase; argon gas was injected at the bottom of the tank to smoothly displace the air exiting at the top.

Large-scale tests at FNAL with a 30-t LAr tank [Liquid Argon Purity Demonstrator project (113)] are under way. The purification of the tank, starting from air, proceeds through three main steps: an initial purge with argon gas, gas recirculation while the tank is heated to 50°C to remove water, and LAr filling and recirculation. Preliminary results (114) are very encouraging; they show electron lifetimes of ~3 ms.

4.3.2. Purification methods. The ICARUS Collaboration (21) has used commercial Oxisorb filters in combination with molecular sieves for argon purification. Regenerable custom-made purification cartridges that employ reduced copper as the purification agent were first used (53) for gas-phase argon and were later successfully operated (115, 116) directly in LAr. Notably, activated copper–coated alumina granules have been employed at FNAL (115). Such cartridges are easily regenerable at ~250°C in a 95:5 mixture of Ar:H_2 gas. Combined with a type 4A upstream molecular sieve filter, electron lifetimes of ~10 ms (at the upper limit of the purity monitor range) have routinely been obtained (115).

4.3.3. Qualification of materials. A facility has been created at FNAL (117) to test several materials commonly used in detector construction. No effect on the electron lifetime was measured when these materials were immersed in LAr, but when they were positioned in the warmer region of the vapor phase (at ~200 K), the electron lifetime strongly decreased; this reduction in electron lifetime correlated with an increase of water concentration in the vapor phase. Water may be responsible for the decrease of the lifetime, and water concentrations in liquid phase at the 10-ppt level may affect the electron lifetime (117).

4.3.4. Monitors of argon purity. An effective way to monitor the attenuation of the ionization charge, which occurs because of electronegative impurities, is to make a three-dimensional reconstruction of cosmic muons in a TPC. From this reconstruction, one can measure the collected charge per unit length versus drift distance. However, it is important to have devices that can perform such measurements both in real time and without relying on the full functionality of the TPC. The purity monitor described in Reference 56 is suitable for electron lifetimes from a few microseconds to a few milliseconds. It was further optimized for use in ICARUS T600 (21).

A novel monitoring and calibration system that exploits UV laser ionization in LAr has been devised (118). Laser-generated tracks can be used to measure the drift velocity and the uniformity of the drift field and to determine the electron lifetime.

UV laser ionization of LAr for TPC calibration was first studied (119) by use of a pulsed UV Nd:YAG laser, which operated on the fourth harmonic with a wavelength of 266 nm, corresponding to 4.66-eV photons. LAr ionization occurs as a multiphoton process wherein a two-photon, near-resonance excitation of an argon atom is followed by absorption of another photon, causing ionization. This mechanism was subsequently studied in Reference 79, which identifies an

important disagreement with the previous measurement (119) of the two-photon excitation cross section; this discrepancy is not yet understood.

The decay time of the slow component (t_{slow}) of LAr scintillation light is very sensitive to the presence of impurities in LAr; its dependence on the concentration of impurities has been studied in References 120 and 121 for contamination by N_2 and O_2, respectively. Measurements of t_{slow} have been used as a simple monitor of impurities, with a sensitivity down to 0.1 ppm (122).

4.4. Detection of Ionization Charge and Scintillation Light

The choice of readout method for the ionization charge released in LAr and the approach used for detection of scintillation light play essential roles in the design of a large LAr TPC.

4.4.1. Charge readout in liquid phase with wire planes. The wire readout technique (5) offers the possibility to acquire three independent views of events in the very stable liquid-phase condition. The LAr density at the normal boiling point changes by $-0.44\%\ K^{-1}$; temperatures are typically stable to much lower than 1 K.

Direct scaling from the ICARUS T600 design to much larger dimensions is not feasible. The mechanical and electrical properties of the wires—namely tension, sagging, the possibility that vibrations will induce microphonic noise, electrical resistance, and capacitance—must be checked and optimized. The total input capacitance to the amplifiers scales with the wire and signal cable lengths and may become a limiting factor in the design due to the worsening of the signal-to-noise ratio (S/N) (123). Typical capacitances are $\sim$20 pF m^{-1} and $\sim$50–100 pF m^{-1} for wires and signal cables, respectively. Input capacitances exceeding 400 pF are expected for 10-m-long wires, when preamplifiers are located outside a large cryostat.

For large-capacitance detectors, the dominant noise is the series noise (voltage noise) of the first transistor of the amplifier; it increases linearly with the input capacitance. In the case of warm electronics, placed outside the cryostat, JFETs are usually employed as the first stage of the amplifiers because of their sufficiently high transconductance and their extremely small parallel noise (current noise) (124, 125). The equivalent noise charge (ENC) of the JFET can be expressed as (123, 124)

$$\mathrm{ENC}^2 = e_{sn}^2 C_{in}^2 / t_p,$$

where $e_{sn}^2 = 4kT(2/3)/g_m$ is the series noise; C_{in} is the total input capacitance, equal to the sum of the wire, signal cable, and input transistor capacitances; and t_p is the shaping time. The basic design of preamplifiers with multiple JFETs at the input stage, connected in parallel to increase the transconductance g_m, was first employed by the ICARUS Collaboration (21) and successfully adopted by other groups (126, 127). The ICARUS T600 amplifier has an ENC of $\sim$1,250 electrons at $C_{in} = 450$ pF (125), which yields an S/N of $\sim$10 in the case of MIPs for 3-mm wire spacing.

In the case of long wires, it is important to use a low-resistivity wire material to limit the input thermal noise to the amplifier (128). For stainless-steel wires, the noise contribution due to the resistivity of the wire becomes important for wire lengths $\gtrsim$5 m. In a novel concept adopted for the LBNE project (106, 123), the LAr volume is filled with a three-dimensional array of TPC cells, with a maximum wire length of $\sim$10 m, and specifically designed front-end electronics operate in LAr next to the wire ends, eliminating the need for long readout cables.

Application-specific integrated circuits (ASICs) based on CMOS technology for front-end applications for LAr TPCs, operating in LAr inside the cryostat, have recently attracted increased

attention (129, 130). Standard test methods are being applied to verify the lifetime of these components (106, 123), which will be required to operate for more than 20 years.

The MicroBooNE experiment (131) has developed a 180-nm CMOS ASIC (132) to be operated in LAr. This ASIC has a power consumption of only ~6 mW per channel. Test results show an ENC that decreases from ~1,200 electrons at 293 K to fewer than 600 electrons at 77 K with 150-pF input capacitance. These results demonstrate the possibility of achieving an ENC smaller than 1,000 electrons for a 10-m-long wire with front-end electronics located in LAr in close proximity to the wire end.

The integration of an analog front-end amplifier with a digitizer in the same ASIC, operated at LAr temperature, is presently being developed (130); the use of both electrical and optical cryogenic digital data links, for the transmission of the signals to the outside of the cryostat, is being investigated (133). Such a solution would substantially reduce the number and complexity of cryogenic feedthroughs.

4.4.2. Scintillation light detection. The ICARUS T600 detector (21) uses tetraphenylbutadiene (TPB)-coated PMTs (66) to shift the ~127-nm LAr scintillation light to the visible region. Recent measurements of the visible reemission spectrum and fluorescence efficiency of TPB, using a TPB film produced by vacuum evaporation, have been reported (134). Under the assumption of a Lambertian angular distribution of the reemitted light from both sides of the TPB film, ~1.2 photons are emitted, in a band centered at ~420 nm, for every 127-nm photon absorbed.

Large-area light-collection systems are needed for large LAr TPCs. One solution (135) uses acrylic light guides coated with a solution of polystyrene and TPB. Multiple bars are bent to adiabatically guide the light to a single PMT, thereby efficiently using the active area of the PMT.

4.4.3. Charge collection and amplification in double phase. A charge-imaging LAr TPC operated in double phase, designated the large electron multiplier time-projection chamber (LEM TPC), was first suggested (24) to improve imaging capabilities and somewhat compensate for charge attenuation in very long drift paths. Ionization electrons drift toward the liquid surface at the top of a vertical cryostat, are then extracted in pure argon gas, and are amplified by thick macroscopic GEMs (gas electron multipliers, also known as THGEMs).

A very active R&D program is being conducted on THGEMs (136), which are macroscopic hole-charge multipliers manufactured with standard printed circuit board techniques. They have been successfully operated in noble gases, without any added quenching gas, and in double-phase argon detectors (137).

The first LEM TPC prototype was successfully operated (126) with a double-stage THGEM of 10×10 cm^2. The amplified charge was read out via two orthogonal coordinates by use of the induced signal on the upper segmented plane of the top THGEM and the collection signal on a segmented anode.

In an improved design (116), to decouple the mechanism of charge amplification in the THGEM from the charge readout, the amplified charge is drifted to a two-dimensional projective readout anode, which provides two independent views with 3-mm spatial resolution. An effective ~30-fold amplification of the released ionization charge has been achieved (116) with a single 10×10 cm^2 THGEM configuration, operated with an electric field of ~35 kV cm^{-1}, without any degradation in resolution; MIPs have been detected with an S/N larger than 200.

The readout of a large-area detector would be realized by an assembly of many independent readout units, each still of a relatively large area of the order of 1 m^2. Recently, a LEM TPC with a readout unit of 76×40 cm^2 was successfully tested (127) with an effective ~14-fold charge amplification.

4.4.4. Charge readout through light. Signals from an ^{55}Fe source were observed (138) with good energy resolution in a double-phase argon setup through detection of the secondary scintillation light produced by the ionization electrons extracted from the liquid and drifted into the holes of a THGEM. This device operated with electric fields of ∼20 kV cm^{-1} in pure argon gas. The scintillation light was detected by a single 1-mm^2 silicon photomultiplier coated with TPB. The application of this technique to large LAr TPCs could be feasible, but it would require substantial R&D on low-cost photosensors. The claim (138) that secondary scintillation light is also observed when a THGEM is operated while immersed in LAr, with fields of ∼60 kV cm^{-1}, has yet to be confirmed.

4.5. Long Electron Drifts

Electron drifts of at least a couple of meters are necessary for the realization of a realistic 10-kt scale LAr detector, even if it is built in a modular way. A 5-m drift device (109) has been constructed for a full-scale demonstration of very long drifts, directly addressing the issues of the generation of very high voltages (up to 500 kV) and the achievable S/N. In the first test (109), performed in 2012, cosmic-muon tracks were observed for drift distances up to 5 m.

5. TOWARD LARGE LIQUID ARGON DETECTORS

Motivated by the necessity of large detectors for neutrino physics, proton decay, and the observation of astrophysical neutrinos, several groups have recently proposed designs of large (up to ∼100 kt) LAr detectors (23–28, 30, 106, 125). **Figure 2** summarizes the main concepts of these designs, which we discuss further in this section.

5.1. Large Evacuable Vessels with Charge Readout in Liquid Phase

Reference 26 proposes scalable detectors, based on a three-dimensional cubic frame array immersed in a common LAr volume (see **Figure 2*a*** for a 3^3 configuration), that have a basic cubic cell of ∼200 m^3 and a drift length of ∼5 m. Such a mechanical structure allows for the evacuation of the inner vessel, so as to preventively check its tightness, but at the expense of complicating the construction and assembly of the readout devices. The design assumes a double-walled cryostat, with vacuum insulation around the cold vessel to optimize thermal insulation.

5.2. Large Nonevacuable Vessels with Charge Readout in Liquid Phase

The MODULAr proposal (27, 125) argues that a tens-of-kilotonnes LAr TPC would be best realized with a modular set of ∼5-kt independent units. The geometry is directly scaled from the ICARUS T600 detector, by a factor of approximately three in each dimension, corresponding to a 4-m drift length (**Figure 2*b***). The wire pitch is 6 mm to compensate for the higher input capacitance due to the longer wires. The vessel is nonevacuable, with 1.5-m-thick perlite walls as passive heat insulation.

The LBNE LAr TPC (106) will consist, in its initial phase, of two stainless-steel membrane cryostats, each of which has a total mass of 9.4 kt of LAr and a fiducial mass of 5 kt. The concept is based on 2.3-m drift double-TPC cells, with one double-sided anode wire plane assembly in the middle and a cathode plane assembly on each side (**Figure 2*c***). The TPC cells, 7 m high and 2.5 m wide in the beam direction, are repeated in three dimensions within the cryostat; there are no constraints on the length of the signal cables thanks to the use of cryogenic electronics. The wire planes provide three independent views with a 4.5-mm wire pitch.

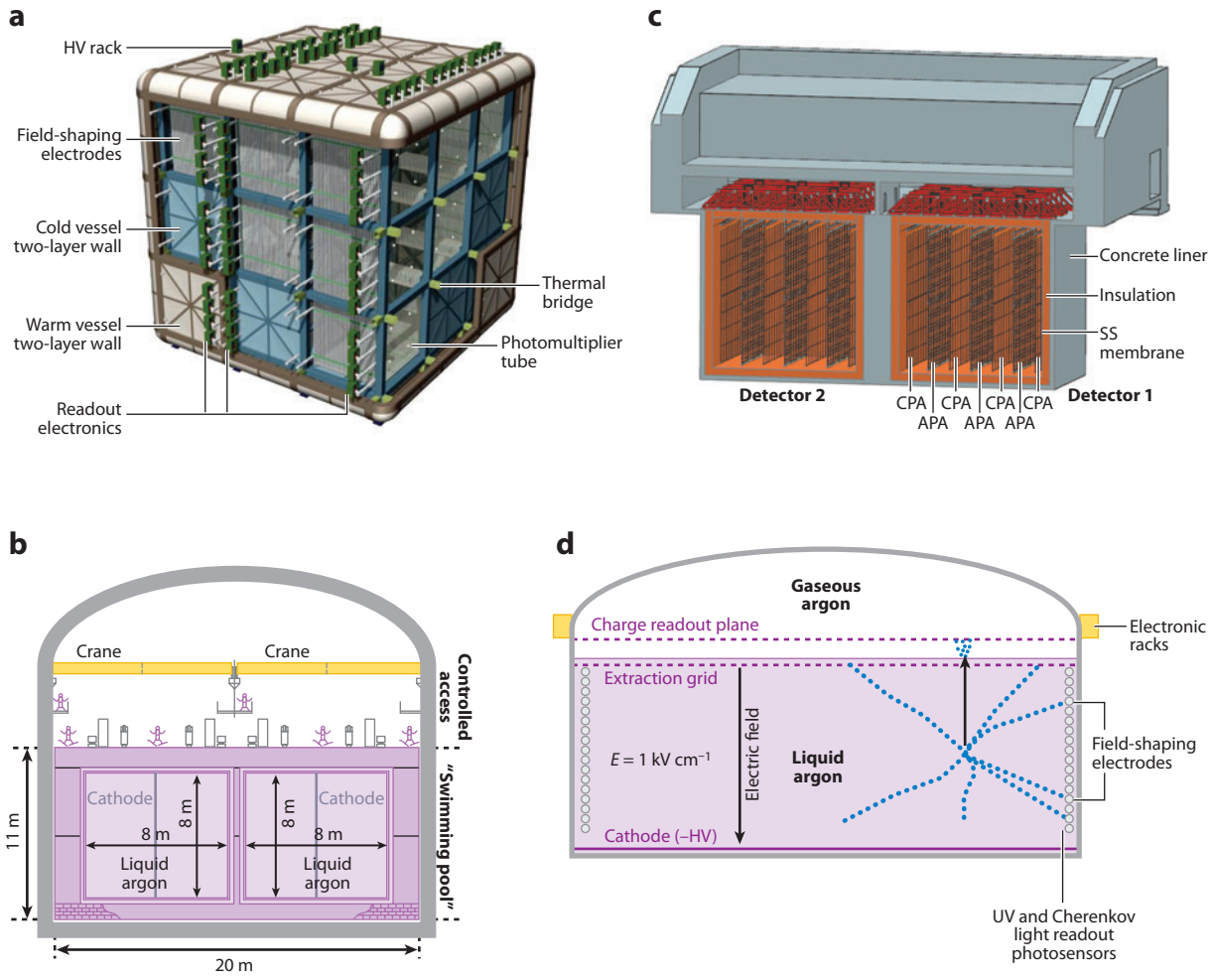

Figure 2

Main design concepts for large liquid argon time-projection chambers. (*a*) An evacuable cryostat with vacuum insulation. Adapted from Reference 26. (*b*) A nonevacuable cryostat with passive insulation, built from 5-kt modules extrapolated from ICARUS. Adapted from Reference 125. (*c*) A nonevacuable cryostat based on membrane cryostat technology, with immersed electronics distributed inside the detector volume (106). (*d*) A nonevacuable cryostat, based on the liquefied natural gas tank design, with vertical drift of the ionization charge and subsequent amplification in pure argon gas at the top. Adapted from Reference 139. Abbreviations: APA, anode wire plane assembly; CPA, cathode plane assembly; HV, high voltage; SS: stainless steel.

5.3. Large Nonevacuable Vessels with Charge Readout in Double Phase

A single 100-kt LAr module, denoted GLACIER, has been proposed (**Figure 2*d***) (24, 28, 139). GLACIER has an almost totally active LAr mass. The vessel, in its original design, is a cylindrical stainless-steel 9%-nickel tank based on industrial LNG technology; its diameter is 70 m and its height is 20 m. The ionization charge is vertically drifted with an electric field of ∼1 kV cm^{-1}, provided by an immersed Cockcroft–Walton voltage multiplier, and collected and amplified in the argon vapor phase (see Section 4.4.3). A 20-kt detector, with 20-m drift, was recently put forward

as the initial phase of the LBNO proposal (30) at CERN. Both a stainless-steel 9%-nickel tank and a membrane cryostat are presently being investigated as options for the LAr vessel.

5.4. Test-Beam Setups and Intermediate-Scale Detectors

Test-beam setups and intermediate-scale detectors are important because they integrate some design aspects of large LAr detectors and complement the bench-type devices (Section 4) that address specific technological points. They enable physics measurements, the development of simulation tools and reconstruction software, and assessments of the performance of LAr detectors (i.e., electron/π^0 separation) in real working conditions. Here, we describe devices that have recently been operated or are presently being built.

ArgoNeuT (140–142), a 170-liter active-volume detector, has been exposed to the NuMI neutrino line at FNAL. It has collected neutrino interactions in the 0.5–10-GeV range. In the near future, the ArgoNeuT detector will be exposed to a low-energy test beam (143) at FNAL to study ionization charge recombination and particle-identification capabilities.

The MicroBooNE detector (131), with a ~60-t fiducial LAr mass, is presently under construction at FNAL and will be located on the Booster neutrino beam line. MicroBooNE will test some of the important design aspects of large LAr TPCs, such as the use of cryogenic electronics in LAr, the achievement of adequate argon purity in a large nonevacuable vessel, operation with a ~2.5-m drift length, and the use of foam as thermal insulation for the cryostat; it will directly measure the uniformity of temperature and drift velocity. This detector will collect more than 100,000 low-energy neutrino interactions, will address cosmic-ray backgrounds to proton decay searches, and will be equipped with a trigger for supernova neutrino detection.

At the J-PARC facility, a 250-liter LAr TPC (144) has been exposed to a 500–800-MeV hadron beam, enriched in kaons. This test will provide particle-identification capabilities in a LAr TPC through the measurement of specific ionization versus residual range for pions, protons, and kaons. It will also provide an estimate of efficiency and background for proton decay searches in the charged kaon decay mode.

6. CONCLUSIONS

The use of LAr TPCs as detectors for neutrinos, both from accelerator beams and astrophysical sources and for rare event searches, has been proposed since the 1970s. A vigorous R&D effort from the ICARUS Collaboration has culminated in the successful operation of the T600 detector at LNGS, Italy.

Several large LAr TPC detectors, based on somewhat different approaches, have been proposed during the past 10 years. Engineering studies have been performed for large cryogenic vessels; they have mostly attempted to adapt industry standards from LNG technology. Experimental tests on LAr purification have been performed, beginning from nonevacuable vessels. Substantial developments in the realization of cryogenic electronics have given rise to designs of large vessels with electronics distributed throughout the volume. A renewed interest in double-phase operation has prompted the development of novel detectors with amplification of the ionization charge in the gas phase. More efficient and cost-effective solutions have been proposed for the detection of scintillation light. The wealth of new developments has allowed us to create comprehensive designs and make reliable cost estimates. The exposure of small- or intermediate-scale LAr TPCs to hadron and neutrino beams, in addition to their specific technical and physics goals, has helped us develop new communities interested in LAr technology, with focused efforts in software and event reconstruction.

DISCLOSURE STATEMENT

The author is not aware of any affiliations, memberships, funding, or financial holdings that might be perceived as affecting the objectivity of this review.

ACKNOWLEDGMENTS

I gratefully acknowledge my many colleagues at ETH Zurich, FNAL, CERN, and KEK for enlightening discussions on liquid argon technology. In particular, I thank Bruce Baller, Stephen Pordes, André Rubbia, and Franco Sergiampietri. Work on this review was supported by the U.S. Department of Energy under contract DE-AC02-07CH11359.

LITERATURE CITED

1. Marshall JH. *Rev. Sci. Instrum.* 25:232 (1954)
2. Alvarez LW. *Lawrence Radiat. Lab. phys. note 672.* **http://alvarezphysicsmemos.lbl.gov/memo.html** (1968)
3. Rubbia C. *The Liquid-Argon Time Projection Chamber: A New Concept for Neutrino Detectors. CERN-EP/77-08*. Geneva, Switz.: CERN (1977)
4. Chen HH, Lathrop JF. *Nucl. Instrum. Methods* 150:585 (1978)
5. Gatti E, et al. *IEEE Trans. Nucl. Sci.* 26:2910 (1979)
6. Shibamura E, et al. *Nucl. Instrum. Methods* 131:249 (1975)
7. Derenzo SE, et al. *Nucl. Instrum. Methods* 122:319 (1974)
8. Miyajima M, et al. *Phys. Rev. A* 9:1438 (1974); Miyajima M, et al. Erratum. *Phys. Rev. A* 10:1452 (1974)
9. Jortner J, Meyer L, Rice SA, Wilson EG. *J. Chem. Phys.* 42:4250 (1965)
10. Hitachi A, et al. *Phys. Rev. B* 27:5279 (1983)
11. Doke T, Masuda K, Shibamura E. *Nucl. Instrum. Methods A* 291:617 (1990)
12. Swan DW. *Proc. Phys. Soc.* 82:74 (1963)
13. Hofmann W, et al. *Nucl. Instrum. Methods* 135:151 (1976)
14. Bakale G, Sowada U, Schmidt WF. *J. Phys. Chem.* 80:2556 (1976)
15. Cennini P, et al. *Nucl. Instrum. Methods A* 333:567 (1993)
16. Bahcall JN, Baldo-Ceolin M, Cline DB, Rubbia C. *Phys. Lett. B* 178:324 (1986)
17. Giboni KL. *Nucl. Instrum. Methods A* 225:579 (1984)
18. ICARUS Collab. *Searching for New Underground Phenomena with High Resolution Visual Techniques and Magnetic Analysis. INFN/AE-85/7*. Frascati, It.: INFN (1985)
19. ICARUS Collab. *ICARUS-I: An Optimized, Real Time Detector of Solar Neutrinos. INFN-LNF-89/005(R)*. Frascati, It.: INFN (1989)
20. ICARUS Collab. *ICARUS-II: A Second Generation Proton Decay Experiment and Neutrino Observatory at the Gran Sasso Laboratory. Proposal*, Vol. I, II. *LNGS-94/99*. Frascati, It.: INFN (1993–1994)
21. Amerio S, et al. *Nucl. Instrum. Methods A* 527:329 (2004)
22. Rubbia C, et al. *J. Instrum.* 6:P07011 (2011)
23. Cline DB, Sergiampietri F, Learned JG, McDonald K. *Nucl. Instrum. Methods A* 503:136 (2003)
24. Rubbia A. arXiv:hep-ph/0402110 (2004)
25. Bartoszek L, et al. (FLARE Collab.) arXiv:hep-ex/0408121 (2004)
26. Cline DB, Raffaelli F, Sergiampietri F. *J. Instrum.* 1:T09001 (2006)
27. Baibussinov B, et al. *Astropart. Phys.* 29:174 (2008)
28. Rubbia A. *J. Phys. Conf. Ser.* 171:012020 (2009)
29. Akiri T, et al. (LBNE Collab.) arXiv:1110.6249 [hep-ex] (2011)
30. Stahl A, et al. *Expression of Interest for a Very Long Baseline Neutrino Oscillation Experiment (LBNO). CERN-SPSC-2012-021*. Geneva, Switz.: CERN (2012)
31. Diwan MV, et al. *Phys. Rev. D* 68:012002 (2003)
32. Bueno A, et al. *J. High Energy Phys.* 04:041 (2007)

33. Gil Botella I, Rubbia A. *J. Cosmol. Astropart. Phys.* 10:009 (2003)
34. Cocco AG, et al. *J. Cosmol. Astropart. Phys.* 12:002 (2004)
35. Rubbia A. *AIP Conf. Proc.* 533:220 (2000)
36. Conrad J, de Gouvêa A, Shalgar S, Spitz J. *Phys. Rev. D* 82:093012 (2010)
37. Ereditato A, Rubbia A. *Nucl. Phys. B Proc. Suppl.* 155:233 (2006)
38. Bueno A, Campanelli M, Rubbia A. *Nucl. Phys. B* 589:577 (2000)
39. Chen H, et al. (MicroBooNE Collab.) *Proposal for a New Experiment Using the Booster and NuMI Neutrino Beamlines. FERMILAB-PROPOSAL-0974.* Batavia, Ill.: Fermi Natl. Accel. Lab. (2007); Chen H, et al. (MicroBooNE Collab.) Addendum to *Proposal for a New Experiment Using the Booster and NuMI Neutrino Beamlines.* Batavia, Ill.: Fermi Natl. Accel. Lab. (2008)
40. Antonello M, et al. arXiv:1203.3432 [physics.ins-det] (2012)
41. Chepel V, Araujo H. *J. Instrum.* 8:R04001 (2013)
42. Davidson N, Larsh AE. *Phys. Rev.* 74:220 (1948)
43. Gerritsen AN. *Physica* 14:407 (1948)
44. Hutchinson GW. *Nature* 162:610 (1948)
45. Davidson N, Larsh AE. *Phys. Rev.* 77:706 (1950)
46. Doke T. *Nucl. Instrum. Methods A* 327:113 (1993)
47. Derenzo SE, et al. *eConf* C700622:45 (1970)
48. Dolgoshein BA, Lebedenko VN, Rodionov BU. *J. Exp. Theor. Phys. Lett.* 11:351 (1970)
49. Dolgoshein BA, et al. *Sov. J. Part. Nucl.* 4:70 (1973)
50. Willis WJ, Radeka V. *Nucl. Instrum. Methods* 120:221 (1974)
51. Blum W, Rolandi L, Riegler W. *Particle Detection with Drift Chambers*. Berlin: Springer (2008)
52. Chen HH, Doe PJ. *IEEE Trans. Nucl. Sci.* 28:454 (1981)
53. Doe PJ, et al. *Nucl. Instrum. Methods A* 258:170 (1987)
54. Aprile E, Giboni KL, Rubbia C. *Nucl. Instrum. Methods A* 241:62 (1985)
55. Buckley E, et al. *Nucl. Instrum. Methods A* 275:364 (1989)
56. Carugno G, Dainese B, Pietropaolo F, Ptohos F. *Nucl. Instrum. Methods A* 292:580 (1990)
57. Doe PJ, Mahler HJ, Chen HH. *Nucl. Instrum. Methods* 199:639 (1982)
58. Bonetti S, et al. *Nucl. Instrum. Methods A* 286:135 (1990)
59. Benetti P, et al. *Nucl. Instrum. Methods A* 332:395 (1993)
60. Cennini P, et al. *Nucl. Instrum. Methods A* 345:230 (1994)
61. Radeka V. *IEEE Trans. Nucl. Sci.* 21:51 (1974)
62. Arneodo F, et al. *Phys. Rev. D* 74:112001 (2006)
63. Baibussinov B, et al. arXiv:1108.3825 [physics.ins-det] (2011)
64. Cennini P, et al. *Nucl. Instrum. Methods A* 432:240 (1999)
65. Benetti P, et al. *Nucl. Instrum. Methods A* 505:89 (2003)
66. Burton WM, Powell BA. *Appl. Opt.* 12:87 (1973)
67. Ankowski A, et al. *Nucl. Instrum. Methods A* 556:146 (2006)
68. Amoruso S, et al. *Nucl. Instrum. Methods A* 516:68 (2004)
69. Antonello M, et al. *Phys. Lett. B* 711:270 (2012)
70. Antonello M, et al. *Phys. Lett. B* 713:17 (2012)
71. Antonello M, et al. *Eur. Phys. J. C* 73:2345 (2013)
72. Zucker MA, Kishore AR, Sukumar R, Dragoset RA, eds. *National Institute of Standards and Technology* (*NIST*) *Elemental Data Index*. Washington, DC: NIST. **http://www.nist.gov/pml/data/edi.cfm** (2011)
73. Benetti P, et al. *Nucl. Instrum. Methods A* 574:83 (2007)
74. Loosli H. *Earth Planet. Sci. Lett.* 63:51 (1983)
75. Linstrom PJ, ed. *National Institute of Standards and Technology* (*NIST*) *Chemistry WebBook*. Washington, DC: NIST. **http://webbook.nist.gov/chemistry** (2012)
76. Tegeler C, Span R, Wagner W. *J. Phys. Chem. Ref. Data* 28:779 (1999)
77. Beringer J, et al. (Part. Data Group) *Phys. Rev. D* 86:010001 (2012)
78. Heindl T, et al. *Europhys. Lett.* 91:62002 (2010)
79. Badhrees I, et al. *New J. Phys.* 12:113024 (2010)
80. Schmidt WF. *IEEE Trans. Electr. Insul.* EI19:389 (1984)

81. Swan DW, Lewis TJ. *Proc. Phys. Soc.* 78:448 (1961)
82. Amey RL, Cole RH. *J. Chem. Phys.* 40:146 (1964)
83. Sinnock AC, Smith BL. *Phys. Rev.* 181:1297 (1969)
84. Seidel GM, Lanou RE, Yao W. *Nucl. Instrum. Methods A* 489:189 (2002)
85. Walkowiak W. *Nucl. Instrum. Methods A* 449:288 (2000)
86. Shibamura E, Takahashi T, Kubota S, Doke T. *Phys. Rev. A* 20:2547 (1979)
87. Kubota S, et al. *Phys. Rev. B* 17:2762 (1978)
88. Doke T, et al. *Nucl. Instrum. Methods A* 269:291 (1988)
89. Ishida N, et al. *Nucl. Instrum. Methods A* 384:380 (1997)
90. Neumeier A, et al. *Eur. Phys. J. C* 72:2190 (2012)
91. Jesse WP, Sadauskis J. *Phys. Rev.* 90:1120 (1953)
92. Scalettar RT, Doe PJ, Mahler HJ, Chen HH. *Phys. Rev. A* 25:2419 (1982)
93. Thomas J, Imel DA. *Phys. Rev. A* 36:614 (1987)
94. Aprile E, Ku WHM, Park J, Schwartz H. *Nucl. Instrum. Methods A* 261:519 (1987)
95. Amoruso S, et al. *Nucl. Instrum. Methods A* 523:275 (2004)
96. Jaffé G. *Ann. Phys.* 42:303 (1913)
97. Onsager L. *Phys. Rev.* 54:554 (1938)
98. Thomas J, Imel DA, Biller S. *Phys. Rev. A* 38:5793 (1988)
99. Doke T, et al. *Nucl. Instrum. Methods* 134:353 (1976)
100. Lowke JJ, Parker JH. *Phys. Rev.* 181:302 (1969)
101. Gushchin EM, Kruglov AA, Obodovskii IM. *Sov. Phys. JETP* 55:860 (1982)
102. Borghesani AF, Carugno G, Cavenago M, Conti E. *Phys. Lett. A* 149:481 (1990)
103. Borghesani AF, Carugno G, Santini M. *IEEE Trans. Electr. Insul.* 26:615 (1991)
104. Fulford NJ, Slatter MD. *Cryogenics* 28:810 (1988)
105. Mulholland GT. *LANND Feasibility Study*. **http://www.hep.princeton.edu/~mcdonald/nufact/mulholland/ELAN_Proposal.pdf** (2002)
106. LBNE Collab. *Conceptual Design Report*, Vol. 4: *The Liquid Argon Detector at the Far Site*. Batavia, Ill.: Fermi Natl. Accel. Lab. **http://lbne2-docdb.fnal.gov/cgi-bin/ShowDocument?docid=4892** (2012)
107. Harris FS. *Cryogenics* 33:772 (1993)
108. Horikawa S, et al. *J. Phys. Conf. Ser.* 308:012027 (2011)
109. Ereditato A, et al. arXiv:1304.6961 [physics.ins-det] (2013)
110. Badertscher A, et al. *J. Instrum.* 7:P08026 (2012)
111. Jaskierny W, et al. *Test of Purging a Small Tank with Argon. FERMILAB-TM-2384-E.* Batavia, Ill.: Fermi Natl. Accel. Lab. **http://lss.fnal.gov/archive/test-tm/2000/fermilab-tm-2384-e.pdf** (2006)
112. Curioni A, et al. *J. Phys. Conf. Ser.* 308:012024 (2011)
113. Rebel B, et al. *J. Phys. Conf. Ser.* 308:012023 (2011)
114. Adamowski M, et al. *Electron Lifetime Measurements at the LAPD*. Batavia, Ill.: Fermi Natl. Accel. Lab. **http://www.fnal.gov/directorate/program_planning/all_experimenters_meetings/special_reports/Tope_LAPD_12_05_11.pdf** (2011)
115. Curioni A, et al. *Nucl. Instrum. Methods A* 605:306 (2009)
116. Badertscher A, et al. *Nucl. Instrum. Methods A* 641:48 (2011)
117. Andrews R, et al. *Nucl. Instrum. Methods A* 608:251 (2009)
118. Rossi B, et al. *J. Instrum.* 4:P07011 (2009)
119. Sun J, Cao D, Dimmock J. *Nucl. Instrum. Methods A* 370:372 (1996)
120. Acciarri R, et al. *J. Instrum.* 5:P06003 (2010)
121. Acciarri R, et al. *J. Instrum.* 5:P05003 (2010)
122. Amsler C, et al. *J. Instrum.* 5:P11003 (2010)
123. Radeka V, et al. *J. Phys. Conf. Ser.* 308:012021 (2011)
124. Radeka V. *Annu. Rev. Nucl. Part. Sci.* 38:217 (1988)
125. Angeli D, et al. *J. Instrum.* 4:P02003 (2009)
126. Badertscher A, et al. arXiv:0811.3384 [physics.ins-det] (2008)
127. Badertscher A, et al. *J. Instrum.* 8:P04012 (2013)

128. Rescia S, Radeka V. In *IEEE Nuclear Science Symposium Conference Record* (*NSS/MIC*), ed. B Yu, p. 1932. Piscataway, N.J.: IEEE (2009)
129. Autiero D, et al. In *Proceedings of the European Strategy for Future Neutrino Physics Workshop*, *CERN Yellow Rep. CERN-2010-003*, ed A Blondel, F Dufour, p. 241, Geneva, Switz.: CERN (2009)
130. De Geronimo G, et al. *IEEE Trans. Nucl. Sci.* 58:1376 (2011)
131. MicroBooNE Collab. *The MicroBooNE Technical Design Report*. Batavia, Ill.: Fermi Natl. Accel. Lab. **http://microboone-docdb.fnal.gov/cgi-bin/ShowDocument?docid=1821** (2012)
132. Chen H, et al. *J. Instrum.* 7:C12004 (2012)
133. Liu T, et al. *J. Instrum.* 7:C01091 (2012)
134. Gehman VM, et al. *Nucl. Instrum. Methods A* 654:116 (2011)
135. Bugel L, et al. *Nucl. Instrum. Methods A* 640:69 (2011)
136. Breskin A, et al. *Nucl. Instrum. Methods A* 598:107 (2009)
137. Buzulutskov A. *J. Instrum.* 7:C02025 (2012)
138. Lightfoot PK, et al. *J. Instrum.* 4:P04002 (2009)
139. Rubbia A. *J. Phys. Conf. Ser.* 375:042058 (2012)
140. Anderson C, et al. *J. Instrum.* 7:P10019 (2012)
141. Anderson C, et al. *Phys. Rev. Lett.* 108:161802 (2012)
142. Anderson C, et al. *J. Instrum.* 7:P10020 (2012)
143. Adamson P, et al. (LArIAT Collab.) *LArIAT: Liquid Argon TPC in a Test Beam. FERMILAB-PROPOSAL-T-1034.* Batavia, Ill.: Fermi Natl. Accel. Lab. (2013)
144. Araoka O, et al. *J. Phys. Conf. Ser.* 308:012008 (2011)

Annual Review of Nuclear and Particle Science

Volume 63, 2013

Contents

Index

Errata

An online log of corrections to *Annual Review of Nuclear and Particle Science* articles may be found at http://nucl.annualreviews.org/errata.shtml